

1 **Marine plastics alter the organic matter composition of the air-sea boundary layer, with**
2 **influences on CO₂ exchange: a large-scale analysis method to explore future ocean**
3 **scenarios**

4 **List of authors:**

5 Luisa Galgani^{1,2,3*}, Eleni Tzempelikou^{4a}, Ioanna Kalantzi^{4b}, Anastasia Tsiola^{4b}, Manolis
6 Tsapakis^{4b}, Paraskevi Pitta^{4b}, Chiara Esposito⁵, Anastasia Tsotskou^{4b}, Iordanis Magiopoulos^{4b},
7 Roberto Benavides³, Tobias Steinhoff³ and Steven A. Loiselle^{1,6}

8 *corresponding author luisa.galgani@unisi.it

9 **Affiliations**

10 ¹Environmental Spectroscopy Group, Department of Biotechnology, Chemistry and Pharmacy,
11 University of Siena, Italy

12 ² (now at) Harbor Branch Oceanographic Institute of Florida Atlantic University, USA

13 ³ (now at) GEOMAR-Helmholtz Centre for Ocean Research Kiel, Germany

14 ^{4a}Institute of Oceanography, Anavyssos, ^{4b}Institute of Oceanography, Heraklion, Hellenic
15 Centre for Marine Research, Greece.

16 ⁵Lake Ecology, Department of Ecoscience and WATEC Aarhus University Centre for Water
17 Technology, Aarhus University, Denmark

18 ⁶Consorzio Interuniversitario Nazionale per la Scienza e Tecnologia dei Materiali, Florence,
19 Italy.

20 **Keywords**

21 Microplastics, *p*CO₂, pH, sea-surface microlayer, mesocosms, marine gel particles, dissolved
22 and particulate organic matter

23 **Abstract**

24 Microplastics are substrates for microbial activity and can influence biomass production. This
25 has potentially important implications in the sea-surface microlayer, the marine boundary layer
26 that controls gas exchange with the atmosphere and where biologically produced organic
27 compounds can accumulate. In the present study, we used six large scale mesocosms to
28 simulate future ocean scenarios of high plastic concentration. Each mesocosm was filled with
29 3 m³ of seawater from the oligotrophic Sea of Crete, in the Eastern Mediterranean Sea. A
30 known amount of standard polystyrene microbeads of 30 µm diameter was added to three
31 replicate mesocosms, while maintaining the remaining three as plastic-free controls. Over the
32 course of a 12-day experiment, we explored microbial organic matter dynamics in the sea-
33 surface microlayer in the presence and absence of microplastic contamination of the underlying
34 water. Our study shows that microplastics increased both biomass production and enrichment
35 of carbohydrate-like and proteinaceous marine gel compounds in the sea-surface microlayer.
36 Importantly, this resulted in a 3% reduction in the concentration of dissolved CO₂ in the
37 underlying water. This reduction was associated to both direct and indirect impacts of
38 microplastic pollution on the uptake of CO₂ within the marine carbon cycle, by modifying the
39 biogenic composition of the sea's boundary layer with the atmosphere.

40 **Introduction**

41 The transition layer between environments is home to many fundamental physical, chemical
42 and biological processes. The sea-surface microlayer (SML) is a millimetre-sized interface
43 between the ocean and the atmosphere (Liss and Duce, 2005). It plays an essential role in
44 ocean-climate feedback by mediating air-sea gas exchange and marine aerosol emission (Wurl
45 et al., 2017). The SML has distinctly different biogeochemical properties with respect to its
46 underlying seawater and it is enriched in both dissolved organic matter (DOM) and particulate

47 organic matter (POM), in particular as carbohydrate-and protein-rich marine gel particles
48 (Engel et al., 2017; Liss and Duce, 2005; Wurl and Holmes, 2008).

49 The two major classes of marine gel particles present in the SML are Transparent Exopolymer
50 Particles (TEP) and Coomassie Stainable Particles (CSP). TEP and CSP give the SML its gel-
51 like composition which is prevalent in most parts of the ocean (Wurl and Holmes, 2008) and
52 support large and diversified microbial communities (Cunliffe and Murrell, 2009; Cunliffe et
53 al., 2011), sensitive to local environmental and meteorological conditions (Rahlff et al., 2017;
54 Zäncker et al., 2018). The enrichment of gel particles and their accompanying microbial life
55 favours the creation of stable surface films that can influence the air-sea fluxes of oxygen and
56 carbon dioxide (Calleja et al., 2013; Rahlff et al., 2019; Wurl et al., 2016).

57 Marine gel particles are derived from extracellular polymeric substances (EPS) released during
58 microbial metabolic functions (Santschi et al., 2021). EPS exist in a continuum of sizes,
59 including colloidal as well as dissolved and particulate fractions (Decho and Gutierrez, 2017;
60 Verdugo, 2012). TEP and CSP are considered a class of EPS (Decho and Gutierrez, 2017)
61 larger than 0.4 μm in relation to the pore size of the filter used for their analysis (Engel, 2009).

62 The microbial release of exopolymers is enhanced on plastic surfaces (Michels et al., 2018),
63 part of the carbon-rich substrates that make up the resulting biofilm (Lear et al., 2021; Zhao et
64 al., 2021). The presence of microplastics in natural and artificial seawater can stimulate the
65 microbial release of DOM, probably due to a higher substrate availability for microbial growth
66 (Boldrini et al., 2021; Galgani et al., 2018), as well as to carbon leachates from plastic that
67 stimulate further microbial activity (Romera-Castillo et al., 2022a; Romera-Castillo et al.,
68 2022b). Likewise, both nanoparticles and microparticles can induce EPS secretion by
69 phytoplankton (Santschi et al., 2021; Shiu et al., 2020). The increased production of organic
70 matter around plastic particles can promote biogenic aggregates formation (Shiu et al., 2020).

71 These aggregates can move to the deep ocean (Galgani and Loisel, 2021) or remain in the
72 SML (Galgani and Loisel, 2019).

73 As plastic particles sustain niches for high microbial activity (Amaral-Zettler et al., 2020;
74 Zettler et al., 2013), one central hypothesis of the present study is that a higher concentration
75 of microplastics in near surface conditions (< 3 m depths) stimulates a higher microbial
76 production of organic matter, adding on to the pool of organic compounds enriching the SML,
77 and thereby modify the air-sea gas exchange properties of this interface.

78 It has been recently shown that seawater exposed plastic debris directly release climate relevant
79 gases like DMS (Savoca et al., 2016), methane and ethylene (Royer et al., 2018), suggesting
80 that significant concentrations of surface plastics may have a direct effect on water-air
81 interactions. It has also been cited that important amounts of plastic can reduce the grazing
82 pressure on phytoplankton in marine regions where nutrients are not a limiting factor, with
83 subsequent anoxic conditions due to a cascade effect of initial high biomass production and
84 degradation of the organic material (Kvale et al., 2021). Since much of the plastic at sea is
85 concentrated in oligotrophic subtropical gyres (North Pacific, North Atlantic), it is expected
86 that this additional carbon biomass on plastics offers a supplementary carbon source able to
87 alter biogeochemical cycles (Zhao et al., 2021). Another key hypothesis of the present study is
88 that high microplastic concentrations would promote high biomass production in oligotrophic
89 conditions.

90 To test both hypotheses, pseudo-marine conditions needed to be created with well-defined and
91 repeatable microplastic concentrations, but large enough to allow for particles aggregation, and
92 for SML organic aggregates interaction with bulk water. Likewise, the experimental conditions
93 should remain relatively stable over the medium term to allow for sampling of individual water
94 masses with no mixing of waters with different microplastic concentrations. This was achieved
95 by six large scale mesocosms, each filled with 3 m³ of oligotrophic seawater from the

96 oligotrophic Sea of Crete. Three of the mesocosms were amended with 30- μm diameter
97 polystyrene microbeads (430 particles per L) and three were plastic-free control mesocosms (<
98 0.5 particles larger than 1 μm per L). Prior to microplastic addition all mesocosms were
99 controlled for uniformity. The SML and underlying water properties were subsequently
100 compared over twelve days after the initial conditions.

101 **Materials and methods**

102 ***Mesocosms set up and SML sampling:*** Six mesocosms with a height of ~ 2.5 m and a diameter
103 of 1.32 m made of transparent polyethylene were gravity-filled with 3- m^3 of coastal seawater
104 pumped from below the surface (2 m) in the bay of Gournes (Sea of Crete). To ensure
105 homogeneity of initial conditions, the water was divided equally in each of the six mesocosm
106 and left overnight. The density of seawater during the experiment was 1.032 ± 0.001 g cm^{-3}
107 with an average salinity of 41.4 ± 1.6 PSU. For the duration of the experiment (12 days), the
108 mesocosms were kept in a 150 m^3 deep concrete tank with circulating seawater maintained at
109 a constant temperature of 20 ± 1 $^{\circ}\text{C}$. Each mesocosm was protected by a clear PVC lid to avoid
110 atmospheric contamination. The first sampling (day 0) occurred the day after the mesocosms
111 were filled. An aqueous solution of 30 μm diameter transparent polystyrene microbeads
112 (Sigma-Aldrich, nr. 84135) with a density of 1.05 g cm^{-3} was added to three mesocosms (MP1-
113 3) after the first sampling (day 1) for a concentration of 430 microplastic L^{-1} , corresponding to
114 about 5.92 $\mu\text{g C L}^{-1}$. The microparticles added were pure analytical standards: polystyrene
115 spheres with a nominal diameter of 30 μm and a calibrated particle diameter of 30.25 ± 0.28 μm
116 based on Coulter Multisizer III (Beckman) measurements provided by Sigma for batch
117 BCBR3704V (see Supplementary Information). Polystyrene beads and polyethylene walls
118 have a negative surface charge at pH above 2.5 (Beneš and Paulenová, 1973), reducing the
119 possibility of attraction between the two materials in experimental conditions. We choose not
120 to clean the mesocosms walls from any possible biofilm formation: we believe that this external

121 procedure could significantly interfere with the parameters measured and be more invasive
122 than the effect of periphyton biofilm formed in a few days, which experimental studies show
123 being negligible for larger radius mesocosm (Chung-Chi and Kemp, 2004). Recent
124 experiments show biofilm formation on PE films after extended incubation times (> 60 and >
125 90 days) (Gupta and Devi, 2020; Han et al., 2020), not comparable to the present experiment.
126 Each mesocosm was continuously gently mixed through a centralized airlift system situated
127 just above the bottom surface to create a homogeneous distribution of the water, as described
128 by Pitta and colleagues (2016). The mixing system was the same in each mesocosm. Mesocosm
129 set up, manipulation, and sampling of the underlying water were conducted daily according to
130 standard methods for mesocosms studies performed at CretaCosmos facility
131 (<https://www.aquacosm.eu/mesocosm/cretacosmos/>) (Pitta et al., 2016; Tsiola et al., 2017b).
132 The sea-surface microlayer (SML) was sampled from each mesocosm early in the morning and
133 prior to bulk water sampling every other day on day 0, day 1, day 3, day 5, day 7, day 9 and
134 day 10, to allow a proper re-establishment of the surface film and minimise disturbance. The
135 SML was sampled simultaneously in each mesocosm with 30 cm x 30 cm silicate glass plates
136 with an effective sampling area of 1800 cm². Glass plates were inserted into the mesocosms
137 perpendicular to the surface and withdrawn at a controlled rate of $\sim 6 \text{ cm s}^{-1}$ as suggested by
138 Carlson (Carlson, 1982). The glass plate approach collects a thinner SML ($\sim 60\text{--}150 \mu\text{m}$) when
139 compared to, e.g., the Garrett screen (150–300 μm) (Garrett, 1965). The glass plate method
140 allowed sampling of sufficient volume for analysis with a minimal dilution of the underlying
141 water. The sample retained on both sides of the plates was removed with a wiper and poured
142 into bottles with the aid of a funnel. The procedure was repeated until the necessary volume
143 for analysis was obtained, tracking the exact number of dips per mesocosm. The first sample
144 was discarded and used to rinse the collecting bottle. Glass plates, collecting bottles, wipers
145 and funnels were acid cleaned (HCl 10 %) and Milli-Q rinsed prior use. To avoid cross-

146 contamination, the control mesocosms and the microplastic-treated mesocosms had different
147 sampling equipment (glass plates, funnels, collection bottles, wipers).

148 The thickness (d , μm) of the sampled SML was estimated as:

$$149 \quad d = V / (A \times n) \quad (1)$$

150 where V is the SML volume collected, i.e., 60–140 mL, A is the sampling area of the glass plate
151 ($A = 1800 \text{ cm}^2$) and n is the number of dips. The apparent thickness of the SML ranged between
152 37 and 72 μm , with an overall mean of $54.7 \pm 9.0 \mu\text{m}$ in agreement to previous studies (Carlson,
153 1982; Engel et al., 2018; Rahlff et al., 2019; Zäncker et al., 2017). The sampling thickness was
154 similar for all mesocosms and sampling days. The samples were immediately processed in the
155 laboratory within maximum 30 minutes after collection.

156 ***Dissolved Inorganic Carbon (DIC) and Total Alkalinity (TA) measurements:*** Following
157 Dickson et al. (2007), seawater was drawn into 500 mL glass bottles using a tube to fill them
158 from bottom to the top. Approximately half of the bottle volume was overflowed and a small
159 headspace (approximately 1% of the bottle volume) was left to allow for water expansion. The
160 samples were fixed by adding 100 μL saturated mercury chloride (HgCl_2) solution thus
161 preventing further biological activity, and stored in the dark at room temperature until analysis.
162 The DIC measurements were performed using a coulometric technique with a SOMMA system
163 (Johnson et al., 1998). The determination of TA was performed by potentiometric titration
164 using a VINDTA system (Mintrop et al., 2000). Certified seawater samples were routinely
165 measured to determine a precision estimated to $2.8 \mu\text{mol kg}^{-1}$ for DIC and $1.8 \mu\text{mol kg}^{-1}$ for
166 TA. ***Dissolved carbon dioxide estimates:*** The partial pressure of carbon dioxide in the
167 mesocosms ($p\text{CO}_2$) as well as pH, CO_3^{2-} , HCO_3^- and CO_2 were calculated from DIC and TA at
168 ambient temperature of $20 \pm 1^\circ\text{C}$ and at sea-level pressure with the CO2SYS program (Pierrot
169 et al., 2006) (<https://cdiac.ess-dive.lbl.gov/ftp/co2sys/>). We applied the equilibrium constants
170 K_1 and K_2 of Lueker et al. (2000) as suggested by Dickson et al. (2007) and Orr et al. (2015)

171 for a wider range of salinity and used a K_{SO_4} value, the dissociation constant for HSO_4^- , of
172 Dickson (1990).

173 ***Dissolved organic carbon (DOC) and chromophoric dissolved organic matter (CDOM):***

174 Samples for DOC were filtered immediately after sampling in duplicate through 0.2 μm
175 polycarbonate membranes and stored cool ($+4^\circ\text{C}$) in pre-combusted glass ampoules until
176 analysis. Concentrations were determined using a Shimadzu TOC-V organic carbon analyser
177 and following the high temperature catalytic oxidation method. The system was standardized
178 prior to analysis using a potassium hydrogen phthalate standard solution. Each sample was
179 injected 3 to 5 times and DOC concentrations were calculated from the average value of three
180 replicates that yielded a relative standard deviation $<2\%$. Analytical precision and accuracy
181 were tested against Deep Atlantic Seawater Reference Material provided by the DOC-CRM
182 program (University of Miami – D.A. Hansell, batch 16); measured values: 0.510-0.580
183 ($n=10$), certified value: 0.516-0.540. Drift correction of the DOC results was applied as needed.
184 Samples for CDOM were filtered immediately after collection in duplicates through 0.2 μm
185 polyether sulfone syringe filters and stored cool ($+4^\circ\text{C}$) in pre-combusted amber glass vials
186 until analysis, which was performed within 4 weeks. The CDOM absorbance spectrum was
187 measured with a Lambda 10 ultraviolet-visible light (UV-Vis) Spectrophotometer (Perkin
188 Elmer) from 210 to 750 nm at 960 nm/min, 1 nm wavelength resolution, and at room
189 temperature ($20^\circ\text{C} \pm 2^\circ\text{C}$). For each analysis, spectra were corrected for baseline, Milli-Q water
190 absorbance and for scattering by subtracting the absorbance values at 730 nm. Absorption
191 coefficients $a(\lambda)$ were calculated from absorbance values after Bricaud et al. (Bricaud et al.,
192 1981). The CDOM absorption spectral slope S (nm^{-1}) was determined by linear regression of
193 log-transformed absorption spectra against the wavelength (Bricaud et al., 1981):

194
$$a(\lambda) = a_0 e^{-S(\lambda-\lambda_0)} \quad (2)$$

195 With $a(\lambda_0)$ being the absorption coefficient at a reference wavelength λ_0 . We used multiple 20-
196 nm wavelength intervals in a stepwise (1 nm) linear regression analysis according to Loiselle
197 et al. (Loiselle et al., 2009). Spectral slope correlates with changes in CDOM due to irradiation
198 (photobleaching), and in the wavelength range 275-295, $S_{(275-295)}$ has been shown to be
199 inversely related with DOM molecular weight (Helms et al., 2008).

200 ***Autotrophic and heterotrophic microorganisms:*** Abundances of autotrophic and
201 heterotrophic microorganisms were measured by flow cytometry. Samples for heterotrophic
202 bacteria were fixed with 25% 0.2 μm -filtered glutaraldehyde (0.5% final concentration),
203 incubated at 4°C for 45 min, flash frozen in liquid nitrogen and stored at -80°C until analysis.
204 Frozen samples were thawed at room temperature and sub-samples were stained for bacterial
205 enumeration with the nucleic-acid stain SYBR Green I (final dilution 4×10^{-4} of the stock
206 solution in Tris-EDTA buffer, pH = 8) and incubated for 10 min in the dark (Marie et al., 1997).
207 The sample fluorescence signal was applied to distinguish high and low DNA content cells.
208 Samples for autotrophic microorganisms were not fixed and were analysed without prior
209 staining, based on their auto-fluorescence signal. A FACSCalibur™ flow cytometer (Becton
210 Dickinson) was used following Tsiola et al. (2017a).

211 ***Marine gels:*** Total area and numbers of gel particles were determined by optical microscopy
212 (Engel, 2009). Ten to fifteen mL of sample were filtered using 0.2 μm Nuclepore membranes
213 (Whatman) and stained with 1 mL Alcian Blue solution for polysaccharidic gels (Transparent
214 Exopolymer Particles, TEP) and 1 mL Coomassie Brilliant Blue G solution for proteinaceous
215 gels (Coomassie Stainable Particles, CSP). Filters were mounted onto CytoClear® slides and
216 stored at -20°C until microscopic analysis. For each slide, thirty images were taken randomly
217 at 200x magnification with a light microscope equipped with a digital camera. The analysis of
218 the cross-sectional area of marine gels was performed with an image analysis software (ImageJ,

219 U.S. National Institutes of Health) and used to calculate the equivalent spherical diameter
220 (ESD) of individual particles, particle number, volume and total area. The size frequency
221 distribution of marine gel particles was determined according to their equivalent spherical
222 diameter, described with a power function of the type:

$$223 \frac{dN}{d(d_p)} = k_p^\delta \quad (3)$$

224 with dN as the number of particles per unit volume in the size range d_p to $[d_p + d(d_p)]$, k a
225 constant which depends on the concentrations of particles, and δ the slope ($\delta < 0$) describing
226 the size distribution. A less negative δ implies an increase in the fraction of larger marine gels.
227 k and δ were both derived from regressions of $\log[dN/d(d_p)]$ versus $\log[d_p]$ (Harlay et al.,
228 2009; Mari and Burd, 1998; Mari and Kiørboe, 1996). The volume concentration of TEP and
229 CSP refers to the mean volume of the particles $> 0.2 \mu\text{m}$ (membrane pore size cut-off); changes
230 in this parameter indicate modifications in particle dynamics such as
231 aggregation/disaggregation processes.

232 Since TEP are considered fractal aggregates, the volume and the carbon content of these marine
233 gel particles are assumed to be proportional to r^D , with r being the equivalent spherical radius
234 (μm) and D the fractal scaling dimension associated with the size-distribution of marine gels
235 (Engel, 2009; Mari and Burd, 1998; Mari and Kiørboe, 1996). TEP carbon content (TEP-C,
236 expressed in $\mu\text{g L}^{-1}$) was determined from marine gel size spectra according to Mari (Mari,
237 1999) and Engel (2009):

$$238 \text{TEP-C } [\mu\text{g L}^{-1}] = 0.25 \times 10^{-6} r^D \quad (4)$$

239 With $D = - 2.55$

240 **Enrichment Factors:** To determine the enrichment or the depletion of each parameter analysed
241 in the SML compared to the underlying water, we determined the Enrichment Factor (EF),
242 defined as:

$$243 \text{EF} = ([X]_\mu / [X]_b) \quad (5)$$

244 With $[X]_{\mu}$, $[X]_b$ the concentration of the specific parameter in the SML (μ) or underlying water
245 (b) (Liss and Duce, 2005). An $EF = 1$ indicates that SML and underlying water values are
246 similar, thus no significant enrichment or depletion in the SML can be observed. While
247 bubbling may have promoted the enrichment of certain compounds in the SML, this process
248 occurred in all mesocosms thus the influence of the airlift mixing system in the comparison of
249 the dynamics of plastic free versus plastic enriched treatments is negligible.

250 **Data analysis and statistics:** To highlight the treatment effect (microplastic addition, MP
251 mesocosms) and avoid the temporal variability, we calculated the normalised anomaly y_{ij} of
252 each mesocosm (j) per day ($i = 0, \dots, 11$) from the overall daily mean of the mesocosms $\bar{y}_i =$
253 $\frac{1}{6} \sum_j^6 (x_j)_i$ following a procedure often applied in mesocosms studies (Endres et al., 2014;
254 Engel et al., 2013):

$$255 \quad y_{ij} = (x_{ij} - \bar{y}_i) / \bar{y}_i \quad (6)$$

256 Differences between control and treated mesocosms were determined by two-tailed unpaired
257 t-tests and Mann-Whitney tests on normalised anomalies, depending on the distribution of the
258 data. Repeated Measures Two-Way ANOVA and Mixed Effects Model (REML) were also
259 used to analyse temporal variations between the control and microplastic treated mesocosms,
260 the latter used in case of missing observations. This method is widely used to analyse data from
261 mesocosms experiments (Dimitriou et al., 2017; Rahav et al., 2016). The fixed factor
262 considered is the treatment (microplastics addition versus control) and the random effect is
263 time (days). Correlations among parameters were determined by Multiple Linear Regression
264 and Spearman correlation analysis. Statistical significance was accepted for $p < 0.05$ and
265 considering a Bonferroni correction for multiple comparisons. All statistical tests were
266 performed with Prism 8.02 (GraphPad Software, San Diego, CA, USA) and Minitab18
267 (Minitab Inc., USA).

268

269 **Results**

270 An earlier study reported an increase in the production of POM and marine gels in the bulk
271 waters of the plastic-amended mesocosms with respect to the plastic-free controls (Galgani et
272 al., 2019). In the present study, we explored differences in the composition of the SML and the
273 possible influence of different SML compositions on the $p\text{CO}_2$ of the underlying bulk water.
274 The SML was analysed for marine gel particles (TEP and CSP), autotrophic and heterotrophic
275 microbial organisms, and dissolved organic matter parameters: Dissolved Organic Carbon,
276 DOC, Chromophoric Dissolved Organic Matter, CDOM, and spectral slope. Salinity, total
277 alkalinity and dissolved inorganic carbon (DIC) were measured from the underlying water and
278 *in-situ* $p\text{CO}_2$, pH, CO_3^{2-} , HCO_3^- and CO_2 were retrieved accordingly. All parameters described
279 in the following paragraphs refer to the SML, except where specified. Biogeochemical
280 processes and relevant data of the underlying water are described in a previous publication
281 (Galgani et al., 2019) and were not the focus of this study.

282 ***Sea surface microlayer dynamics and underlying water $p\text{CO}_2$***

283 Microplastic-amended mesocosms (MP) had significantly lower values of $p\text{CO}_2$ in the
284 underlying water and higher pH compared to control mesocosms (Figure 1). Mean values of
285 $p\text{CO}_2$ in the MP treatments were 3% lower than those found in control mesocosms,
286 corresponding to an increase of 0.14% in pH units (Table 1). Total alkalinity (TA) and
287 dissolved inorganic carbon (DIC) were also significantly higher in the underlying water of MP
288 treatments (Figure 2 and S1). Similar differences were found for estimated concentrations of
289 CO_3^{2-} and CO_2 , with higher CO_3^{2-} in MP treatments (Figure 2).

290 Higher concentrations of both polysaccharidic TEP and proteinaceous CSP were measured in
291 the SML of the MP treated mesocosms (Figure 1, Table 1). A 30% increase in TEP and relative
292 carbon content (TEP-C) along with higher concentrations and particle abundances of both
293 marine gels occurred in the SML of the MP mesocosms, with a mean \pm SEM (standard error of

294 means) TEP-C of $424.8 \pm 58.5 \mu\text{g C L}^{-1}$ compared to $324.3 \pm 42.9 \mu\text{g C L}^{-1}$ in control mesocosms
295 (Figure 1). This was accompanied by a 1% increase in *Synechococcus*, and by a 23% increase
296 of high-DNA containing *Synechococcus* cells in the SML (Figures 1 and S2, Table 1), likely
297 to be the main source of TEP for the whole system. In the underlying water of the mesocosms,
298 an initial (and rapidly declined) phytoplankton bloom was attributed to the presence of
299 autotrophic picoeukaryotes, while *Synechococcus* growth showed a constant increase and
300 represented the dominant species in the mesocosms. This was expected as this species
301 dominates in the oligotrophic waters of the Sea of Crete at this time of the year (Galgani et al.,
302 2019). Heterotrophic bacteria concentrations in the SML were similar in MP and control
303 mesocosms, and significant differences were observed over time rather than across treatments
304 (Figure S2, Table 1). Their concentrations were negatively correlated to those of *Synechococcus*,
305 indicating a potential competition within the highly dynamic environment of the SML
306 (Spearman $r = -0.40$, $p = 0.015$, $n = 37$). Alternating influence of primary and secondary
307 production in the SML was also evidenced in the dynamics of the spectral slope $S_{275-295}$ of the
308 chromophoric dissolved organic matter (CDOM) pool. Higher $S_{275-295}$ is associated to lower
309 molecular weight CDOM often resulting from degradation processes, while lower $S_{275-295}$
310 characterises the “fresh” production of higher molecular weight CDOM (Helms et al., 2008).
311 While DOC and CDOM measured as the absorption coefficient at 355 nm were similar between
312 control and MP mesocosms and significant variations were observed over time (Table 1, Figure
313 S3), $S_{275-295}$ instead was higher in the SML of MP mesocosms (Table 1, Figure S3) confirming
314 that there were significant differences in the DOM production and degradation processes
315 between treatments. In the SML, we observed a strong negative correlation between
316 *Synechococcus* and $S_{275-295}$ (Table 2) as to indicate a release of organic matter from
317 *Synechococcus* cells, and a weaker positive correlation between heterotrophic bacteria and S_{275-}
318 $_{295}$, suggesting a bacterial degradation of organic compounds. $S_{275-295}$ was positively correlated

319 to CSP ($\text{mm}^2 \text{L}^{-1}$), DOC, and $p\text{CO}_2$ (Table 2) hinting to different production dynamics of CSP
320 with respect to TEP and linking CSP concentration to organic matter degradation. In the SML,
321 the amount of TEP-C was weakly related to the abundance of *Synechococcus* (Linear
322 Regression $R^2=0.12$, $p = 0.03$) pointing to a local source (i.e., within the SML) of fresh
323 biological production for this class of marine gel compounds. A positive correlation between
324 DOC and $S_{275-295}$ suggested that the pool of DOC in the SML of the mesocosms is mostly
325 composed of degraded or reworked material, and unlikely linked to a fresh biomass production.
326 Most importantly, we observed significant correlations between the $p\text{CO}_2$ in the underlying
327 water (as well as pH, TA, DIC, CO_3^{2-} and CO_2) with the concentration of TEP-C and
328 *Synechococcus* cells in the SML (Table 3). $p\text{CO}_2$ decreased with increasing TEP concentration
329 and carbon content (Figures 3 and S4a). Instead, CSP in the SML had the opposite relationship
330 with $p\text{CO}_2$ with respect to TEP (Figure 3). This was further demonstrated in the linear
331 relationship between $p\text{CO}_2$ and gel concentrations (Equation 7):

$$332 \quad p\text{CO}_2 [\mu\text{atm}] = 413.189 - 0.0509 \text{ TEP} [\text{mm}^2 \text{L}^{-1}] + 0.04708 \text{ CSP} [\text{mm}^2 \text{L}^{-1}] \quad (7)$$

$$333 \quad R^2 = 0.38, \quad p < 0.001, \quad F=11.98$$

334 It should be noted that underlying water TEP and CSP concentrations from the same
335 experiment did not show any relation to $p\text{CO}_2$. Together with SML gel concentrations, $p\text{CO}_2$
336 in the underlying water was related to SML $S_{275-295}$ and SML *Synechococcus* abundance
337 (Figures S4b, S4c and Tables 2 and 3), indicating the relationship of $p\text{CO}_2$ to different phases
338 of organic matter cycling.

339 ***Sea surface microlayer enrichment and relation to underlying water parameters***

340 In this experiment, the SML represented an enriched environment with respect to the bulk
341 water conditions (Figure 4). *Synechococcus* in the SML was strongly related to the underlying
342 water cell abundances (Spearman $r = 0.945$, $p < 0.0001$, $n = 39$), as well as the amount of
343 CDOM (Spearman $r = 0.859$, $p < 0.0001$, $n = 42$), the latter pointing to similar dynamics in

344 DOM turnover between SML and underlying water. TEP concentration ($\text{mm}^2 \text{L}^{-1}$) in the SML
345 also showed a low but significant relation to underlying water TEP to some extent (Spearman
346 $r = 0.359$, $p = 0.0197$, $n = 42$), confirming that most of the TEP variability in the SML was
347 probably associated to *Synechococcus* cell abundances rather than to the underlying water TEP
348 concentration.

349 Particularly high enrichment factors were observed for marine gels in the SML in all
350 mesocosms, as expected. However, the enrichment factors for TEP and CSP were significantly
351 higher in the MP mesocosms with respect to plastic-free controls (Figure 5, Table S1)
352 indicating that the SML of the mesocosms where plastic was added had a higher accumulation
353 of marine gels (TEP and CSP) with respect to plastic-free controls.

354 **Discussion**

355 The twelve-day experiment coincided with a *Synechococcus* bloom phase in all six mesocosms,
356 during which autotrophic production of particulate organic matter prevailed over heterotrophic
357 production. In the MP mesocosms there was an increased abundance of *Synechococcus* in the
358 underlying water, which dominated over autotrophic picoeukaryotes cell numbers by an order
359 of magnitude (Galgani et al., 2019). Microbial attachment on particles is a common
360 phenomenon in aquatic ecosystems (Paerl, 1975) and microplastics may serve as a physical
361 support for different microorganisms (Zettler et al., 2013; Zhao et al., 2021) creating hot spots
362 of high metabolic activity (Dang and Lovell, 2015).

363 *Synechococcus* is an important primary producer in the Sea of Crete and a known TEP producer
364 also in nutrient-limiting conditions (Deng et al., 2016; Ortega-Retuerta et al., 2019). Globally,
365 *Synechococcus* contributes to 21% of total CO_2 fixation (Jardillier et al., 2010).

366 We hypothesize that two concurrent processes led to the increased accumulation of TEP in the
367 sea-surface microlayer of the mesocosms containing MPs. Firstly, in the MP mesocosms, an
368 increase in *Synechococcus* production led to higher TEP accumulation in the underlying water

369 and enrichment in the SML possibly by migration of these compounds to the surface. The
370 relationship between underlying water and SML gel particles is not novel in field (Engel and
371 Galgani, 2016) and mesocosms studies (Galgani et al., 2014), since the SML partly reflects the
372 underlying water composition. Secondly, *Synechococcus* cells can produce TEP directly in the
373 SML (Yue et al., 2018) and their increased concentration in the SML in the mesocosms
374 containing MPs might have been an additional source for TEP accumulation.

375 In the ocean, TEP aggregation is proved to be a sink for marine carbon (Engel et al., 2004) and
376 natural plankton communities are stimulated to produce TEP as a response to increased CO₂
377 (Engel, 2002). It has also been shown that microbial activity in the sea-surface microlayer can
378 control the exchange rate of atmospheric CO₂ (Calleja et al., 2005); in our experiment, the
379 higher TEP accumulation in the SML of the MP mesocosms may have served as a sink for CO₂
380 as described in equation (7).

381 To further support this difference, DIC partitioning in the underlying water of MP mesocosms
382 had higher CO₃²⁻ and lower CO₂ concentrations with respect to plastic-free controls. This
383 observation might be explained by the fact that *Synechococcus* has also been associated to
384 “whiting” events in marine and lakes environments (Dittrich et al., 2003; Thompson et al.,
385 1997). Whiting events occur when carbonates of biogenic origin are precipitated by
386 microorganisms like cyanobacteria through photo-and chemosynthetic autotrophy in the
387 presence of Mg(2+) and Ca(2+) counterions (Dittrich et al., 2003; Thompson, 2000; Thompson
388 et al., 1997). Many bacteria species are implicated in CaCO₃ precipitation, which represents a
389 potential mechanism for CO₂ sequestration and generally occurs at high pH, during active
390 photosynthesis, and when DIC is limiting, such as after a bloom (Callieri, 2017). During the
391 twelve-day experiment, the highest abundance of *Synechococcus* in the SML and underlying
392 water appeared after the picoeukaryote and heterotrophic blooms (Galgani et al., 2019),
393 corresponding to a migration and enrichment of organic compounds to the SML.

394 In particular, the enrichment of organic particles (i.e. TEP and CSP) in the SML of MP
395 mesocosms led to the establishment of a highly enriched surface film, potentially able to
396 modify gas exchange between the mesocosms and the surrounding atmosphere. The different
397 partitioning of DIC between CO_3^{2-} and CO_2 in MP treatments confirms an increased autotrophy
398 in MP mesocosms that led to lower $p\text{CO}_2$ beneath. In control mesocosms, heterotrophy did not
399 increase, rather, autotrophic production was less as additional substrates for growth and
400 metabolism, elsewhere provided by microplastics, were missing. This led to an overall lower
401 production of marine gels in the underlying water and consequently in the SML, resulting in a
402 less enriched surface film allowing for an increased exchange of atmospheric CO_2 at the air-
403 sea interface. This is similar to the presence of surfactants in the sea-surface microlayer, where
404 the resulting laminar diffusion layer reduces gas transfer (Frew, 1997). Some biogenic
405 surfactants and surface slicks carrying a high microbial biomass can reduce air-sea CO_2
406 exchange by 15% to 19% (Mustaffa et al., 2020; Wurl et al., 2016).

407 While initially $p\text{CO}_2$ concentration might have been lower in the MP mesocosms, we should
408 note that SML enrichment does not only limit the exchange of atmospheric CO_2 , but also that
409 of oxygen across the air-sea interface. In the post-bloom phase dominated by the heterotrophic
410 remineralisation of organic matter, CO_2 is put back into the system through microbial
411 respiration, while oxygen concentrations are reduced. This may be especially important in
412 coastal, shallow and semi-enclosed marine areas affected by plastic and other types of organic
413 or nutrient pollution that favour high autotrophic biomass production. In areas where
414 zooplankton feed on plastic particles because of high plastic concentration, grazing pressure
415 on primary producers is reduced, further increasing autotrophic biomass in eutrophic waters,
416 where the subsequent remineralisation of organic matter can further reduce oxygen
417 concentrations (Kvale et al., 2021).

418 Our study shows that microplastics can increase the accumulation of marine gel particles in the
419 SML by a 25-30% compared to plastic-free conditions. By using large scale mesocosms, it was
420 possible to explore daily changes in SML formation and the resulting impact on the underlying
421 water $p\text{CO}_2$. This supports a better understanding of localized anoxic or hypoxic zones often
422 observed in estuarine and upwelling areas where the SML plays an essential role in air-sea gas
423 exchange (Engel and Galgani, 2016; Hepach et al., 2016; Upstill-Goddard, 2006) and where
424 marine plastisphere communities can have direct effect on the concentration of N_2O and CO_2
425 (Cornejo-D'Ottone et al., 2020; Su et al., 2022).

426 While this method demonstrated the indirect effect of plastics on seawater $p\text{CO}_2$ concentration
427 through the SML, another effect that should be considered is the direct impact on the
428 production and response of marine gels in the SML. TEP and CSP are distinct, insoluble
429 macromolecules derived from the aggregation and annealing of DOM polymeric precursors
430 produced during microbial growth and metabolism (Cisternas-Novoa et al., 2015; Engel, 2009;
431 Thornton, 2018; Thornton et al., 2016). TEP concentrations in the SML were only partly related
432 to those of the underlying water, indicating that an additional source of TEP may be the SML
433 itself through the microbial activity of *Synechococcus*. As such, the SML may act as a direct
434 sink of atmospheric CO_2 through extracellular polymers production within this layer. CSP
435 instead seemed to be more clearly related to the degradation of organic matter present in the
436 SML, as CDOM and $S_{275-295}$ measurements indicated their higher lability and rapid turnover
437 (Thornton, 2018). This creates a pool of organic matter in the SML that is completely
438 independent from underlying water processes, a phenomenon observed in highly productive
439 marine regions (Galgani and Engel, 2016; Zäncker et al., 2017).

440 In the present study, we choose to use polystyrene as it is a very abundant microplastic polymer
441 in oligotrophic marine areas (Pabortsava and Lampitt, 2020). While a recent study has reported
442 that virgin laboratory grade polymer and commercially available polystyrene leaches dissolved

443 organic carbon (DOC) in natural freshwater when exposed to dark and light conditions (Lee et
444 al., 2020), such quantifiable DOC leachate was achieved at elevated concentrations of 5 g L⁻¹,
445 or 10⁶ times higher than the concentration used in the present study (6 x 10⁻⁶ g L⁻¹).

446 The size of microplastics selected for use in the experiment allowed for the comparison to other
447 studies on the influence of microplastics on marine biological processes like zooplankton
448 ingestion (Cole et al., 2013; Cole et al., 2016) and human health (Hwang et al., 2020).
449 Furthermore, the size range and concentration of the polystyrene particles were selected to
450 minimise potential interference with spectrophotometric measurements of dissolved organic
451 matter (Galgani et al., 2018), while allowing for them to be embedded into exopolymer gels in
452 the field (Galgani et al., 2022).

453 It should be noted that the concentration of plastic particles used in this study was higher than
454 typical marine conditions and more similar to those of impacted sediments in coastal areas
455 (Sharma et al., 2021) and projections of future scenarios. While microplastics range between 1
456 µm and 5 mm (Andrady, 2011), most measurements of surface microplastics rely on net tows
457 with a limited mesh size, typically 330 µm (GESAMP, 2019). Therefore, microplastics smaller
458 than 330 µm are largely under-sampled (Zhao et al., 2021), while being those most abundant,
459 due to continuous plastic fragmentation processes. A recent study reported concentrations over
460 ~8000 particles per L in the < 333 µm size fraction (Brandon et al., 2020). Similarly, high
461 concentrations of microplastics (10⁵ particles m⁻³) have been already found in a Swedish
462 harbour in proximity of a plastic manufacture plant (Lindgren et al., 2016).

463 **Conclusions**

464 This mesocosm study shows an important new impact of plastic pollution on marine carbon
465 biogeochemistry, that is the capacity of microplastics to directly influence processes at the air-
466 sea boundary layer, in particular the ocean-atmosphere exchange of CO₂. Although not
467 comparable to field observations, to the best of our knowledge, this experiment is the first to

468 focus on the impacts of plastic on the sea-surface microlayer in a near natural setting, as *in situ*
469 conditions of temperature, irradiation, and natural seawater biological and chemical
470 composition were maintained.

471 Our results show that plastic pollution of the underlying water enhances the production and
472 accumulation of two important classes of marine gels (polysaccharidic, TEP, versus
473 proteinaceous, CSP) in the SML, with important repercussions on the control over the ocean's
474 gas exchange with the atmosphere. Both indirect impacts, through an enriched surface film, as
475 well as direct impacts, through an increase in the remineralisation of organic matter in the SML
476 appear to be active. These results support the growing attention on the influence of plastic on
477 the marine biological carbon pump and therefore on the ocean's capability to store
478 anthropogenic CO₂ (Galgani and Loiselle, 2021; Kvale et al., 2021; Shen et al., 2020). Further
479 efforts should be made to explore these dynamics across different marine environments and
480 trophic regimes. Plastic production is expected to double in the next decades (Borrelle et al.,
481 2020). In the absence of efficient management practices, plastic will continue to accumulate in
482 our oceans and environment. Clearly, the impacts of plastic pollution on marine
483 biogeochemistry go further than what explored in the present study. This highlights the
484 importance of mesocosm-based studies and large-scale ocean simulations to better explore
485 these dynamics, providing needed information to support international agreements to address
486 climate change and the functionality of the oceanic carbon sink (Cooley et al., 2019).

487 **Acknowledgements**

488 We greatly acknowledge G. Piperakis for the setting up of the mesocosms and for his technical
489 assistance throughout the experiment. K. Mylona, I. Santi, S. Zivanovic, E. Dafnomili, S.
490 Diliberto, and A. Loiselle are greatly acknowledged for technical support.

491 **Author contributions:** L.G. designed the experiment in consultation with S.A.L., M.T. and
492 P.P., analysed the data in consultation with S.A.L. and wrote the manuscript. L.G., E.T., I.K.,

493 A.T., M.T., P.P., C.E., A.T., I.M., and S.A.L. contributed to set up and experiment running,
494 samples analysis and manuscript editing. R.B. and T.S. contributed to samples analysis and
495 manuscript editing.

496 **Funding:** This work received funding from the European Union's Horizon 2020 Research and
497 Innovation Programme under the Marie Skłodowska-Curie grant agreement No. 702747 –
498 *POSEIDOMM*, to L. Galgani.

499 **Competing Interests:** The authors declare no competing interests.

500 **Data availability:** all data will be made available on an open repository after publication in
501 conformity with the requirements of all Horizon 2020 funded research projects.

502 **References**

503 Amaral-Zettler, L. A., Zettler, E. R., & Mincer, T. J. (2020). Ecology of the plastisphere. *Nat. Rev.*
504 *Microbiol.*, 18(3), 139-151. <https://doi.org/10.1038/s41579-019-0308-0>

505 Andrady, A. L. (2011). Microplastics in the marine environment. *Mar. Pollut. Bull.*, 62(8), 1596-1605.
506 <https://doi.org/https://doi.org/10.1016/j.marpolbul.2011.05.030>

507 Beneš, P., & Paulenová, M. (1973). Surface charge and adsorption properties of polyethylene in
508 aqueous solutions of inorganic electrolytes. *Kolloid-Zeitschrift und Zeitschrift für Polymere*,
509 251(10), 766-771. <https://doi.org/10.1007/BF01499104>

510 Boldrini, A., Galgani, L., Consumi, M., & Loiselle, S. A. (2021). Microplastics Contamination versus
511 Inorganic Particles: Effects on the Dynamics of Marine Dissolved Organic Matter.
512 *Environments*, 8(3), 21. <https://doi.org/https://doi.org/10.3390/environments8030021>

513 Borrelle, Stephanie B.; Ringma, Jeremy; Law, Kara Lavender; Monnahan, Cole C.; Lebreton, Laurent;
514 McGivern, Alexis; Murphy, Erin; Jambeck, Jenna; Leonard, George H.; Hilleary, Michelle A.;
515 Eriksen, Marcus; Possingham, Hugh P.; De Frond, Hannah; Gerber, Leah R.; Polidoro, Beth;

516 Tahir, Akbar; Bernard, Miranda; Mallos, Nicholas; Barnes, Megan; Rochman, Chelsea M.
517 (2020). Predicted growth in plastic waste exceeds efforts to mitigate plastic pollution. *Science*,
518 369(6510), 1515–1518. doi:10.1126/science.aba3656

519 Brandon, J.A., Freibott, A. and Sala, L.M. (2020), Patterns of suspended and salp-ingested microplastic
520 debris in the North Pacific investigated with epifluorescence microscopy. *Limnol. Oceanogr.*
521 *Lett.*, 5: 46-53. <https://doi.org/10.1002/lol2.10127>

522 Bricaud, A., Morel, A., & Prieur, L. (1981). Absorption by dissolved organic matter of the sea (yellow
523 substance) in the UV and visible domains. *Limnol. Oceanogr.*, 26, 43-53.
524 <https://doi.org/https://doi.org/10.4319/lo.1981.26.1.0043>

525 Calleja, M. L., Duarte, C. M., Álvarez, M., Vaquer-Sunyer, R., Agustí, S., & Herndl, G. J. (2013).
526 Prevalence of strong vertical CO₂ and O₂ variability in the top meters of the ocean. *Global*
527 *Biogeochem. Cycles*, 27(3), 941-949. <https://doi.org/10.1002/gbc.20081>

528 Calleja, M. L., Duarte, C. M., Navarro, N., & Agustí, S. (2005). Control of air-sea CO₂ disequilibria in
529 the subtropical NE Atlantic by planktonic metabolism under the ocean skin. *Geophys. Res.*
530 *Lett.*, 32(8). <https://doi.org/https://doi.org/10.1029/2004GL022120>

531 Callieri, C. (2017). Synechococcus plasticity under environmental changes. *FEMS Microbiol. Lett.*,
532 364(23). <https://doi.org/10.1093/femsle/fnx229>

533 Carlson, D. J. (1982). Phytoplankton in marine surface microlayers. *Can. J. Microbiol.*, 28(11), 1226-
534 1234. <https://doi.org/10.1139/m82-183>

535 Chung-Chi, C., & Kemp, W. M. (2004). Periphyton communities in experimental marine ecosystems:
536 scaling the effects of removal from container walls. *Mar. Ecol. Prog.*, 271, 27-41.
537 <https://www.int-res.com/abstracts/meps/v271/p27-41/>

538 Cisternas-Novoa, C., Lee, C., & Engel, A. (2015). Transparent exopolymer particles (TEP) and
539 Coomassie stainable particles (CSP): Differences between their origin and vertical distributions
540 in the ocean. *Mar. Chem.*, *175*, 56-71.
541 <https://doi.org/https://doi.org/10.1016/j.marchem.2015.03.009>

542 Cole, M., Lindeque, P., Fileman, E., Halsband, C., Goodhead, R., Moger, J., & Galloway, T. S. (2013).
543 Microplastic Ingestion by Zooplankton. *Environ. Sci. Technol.*, *47*(12), 6646-6655.
544 <https://doi.org/10.1021/es400663f>

545 Cole, M., Lindeque, P. K., Fileman, E., Clark, J., Lewis, C., Halsband, C., & Galloway, T. S. (2016).
546 Microplastics Alter the Properties and Sinking Rates of Zooplankton Faecal Pellets. *Environ.*
547 *Sci. Technol.*, *50*(6), 3239-3246. <https://doi.org/10.1021/acs.est.5b05905>

548 Cooley, S. R., Bello, B., Bodansky, D., Mansell, A., Merkl, A., Purvis, N., Ruffo, S., Taraska, G.,
549 Zivian, A., & Leonard, G. H. (2019). Overlooked ocean strategies to address climate change.
550 *Glob. Environ. Change*, *59*, 101968.
551 <https://doi.org/https://doi.org/10.1016/j.gloenvcha.2019.101968>

552 Cornejo-D'Ottone, M., Molina, V., Pavez, J., & Silva, N. (2020). Greenhouse gas cycling by the
553 plastisphere: The sleeper issue of plastic pollution. *Chemosphere*, *246*, 125709.
554 <https://doi.org/https://doi.org/10.1016/j.chemosphere.2019.125709>

555 Cunliffe, M., & Murrell, J. C. (2009). Eukarya 18S rRNA gene diversity in the sea surface microlayer:
556 implications for the structure of the neustonic microbial loop. *ISME J.*, *4*(3), 455-458.
557 <https://doi.org/10.1038/ismej.2009.133>

558 Cunliffe, M., Upstill-Goddard, R. C., & Murrell, J. C. (2011). Microbiology of aquatic surface
559 microlayers. *FEMS Microbiol. Rev.*, *35*(2), 233-246. [https://doi.org/10.1111/j.1574-](https://doi.org/10.1111/j.1574-6976.2010.00246.x)
560 [6976.2010.00246.x](https://doi.org/10.1111/j.1574-6976.2010.00246.x)

- 561 Dang, H., & Lovell, C. R. (2015). Microbial Surface Colonization and Biofilm Development in Marine
562 Environments. *Microbiol. Mol. Biol. Rev.: MMBR*, 80(1), 91-138.
563 <https://doi.org/10.1128/MMBR.00037-15>
- 564 Decho, A. W., & Gutierrez, T. (2017). Microbial Extracellular Polymeric Substances (EPSs) in Ocean
565 Systems. *Front. Microbiol.*, 8. <https://doi.org/10.3389/fmicb.2017.00922>
- 566 Deng, W., Cruz, B. N., & Neuer, S. (2016). Effects of nutrient limitation on cell growth, TEP production
567 and aggregate formation of marine *Synechococcus*. *Aquat. Microb. Ecol.*, 78(1), 39-49.
568 <https://www.int-res.com/abstracts/ame/v78/n1/p39-49/>
- 569 Dickson, A. G. (1990). Standard potential of the reaction: $\text{AgCl(s)} + 12\text{H}_2\text{(g)} = \text{Ag(s)} + \text{HCl(aq)}$, and
570 and the standard acidity constant of the ion HSO_4^- in synthetic sea water from 273.15 to 318.15
571 K. *J. Chem. Thermodyn.*, 22(2), 113-127. [https://doi.org/https://doi.org/10.1016/0021-](https://doi.org/https://doi.org/10.1016/0021-9614(90)90074-Z)
572 [9614\(90\)90074-Z](https://doi.org/https://doi.org/10.1016/0021-9614(90)90074-Z)
- 573 Dickson, A. G., Sabine, C. L., & Christian, J. R. E. (2007). *Guide to Best Practices for Ocean CO2*
574 *Measurements*. PICES Special Publication 3, 191 pp. [https://www.ncei.noaa.gov/access/ocean-](https://www.ncei.noaa.gov/access/ocean-carbon-acidification-data-system/oceans/Handbook_2007.html)
575 [carbon-acidification-data-system/oceans/Handbook_2007.html](https://www.ncei.noaa.gov/access/ocean-carbon-acidification-data-system/oceans/Handbook_2007.html)
- 576 Dimitriou, P. D., Papageorgiou, N., Geropoulos, A., Kalogeropoulou, V., Moraitis, M., Santi, I.,
577 Tsikopoulou, I., Pitta, P., & Karakassis, I. (2017). A novel mesocosm setup for benthic-pelagic
578 coupling experiments. *Limnol. Oceanogr. Meth.*, 15(4), 349-362.
579 <https://doi.org/https://doi.org/10.1002/lom3.10163>
- 580 Dittrich, M., Müller, B., Mavrocordatos, D., & Wehrli, B. (2003). Induced Calcite Precipitation by
581 Cyanobacterium *Synechococcus*. *Acta Hydrochim. Hydrobiol.*, 31(2), 162-169.
582 <https://doi.org/https://doi.org/10.1002/ahch.200300486>

- 583 Endres, S., Galgani, L., Riebesell, U., Schulz, K.-G., & Engel, A. (2014). Stimulated Bacterial Growth
584 under Elevated pCO₂: Results from an Off-Shore Mesocosm Study. *PLOS ONE*, 9(6), e99228.
585 <https://doi.org/10.1371/journal.pone.0099228>
- 586 Engel, A. (2002). Direct relationship between CO₂ uptake and transparent exopolymer particles
587 production in natural phytoplankton. *J. Plankton Res.*, 24(1), 49-53.
588 <https://doi.org/10.1093/plankt/24.1.49>
- 589 Engel, A. (2009). Determination of Marine Gel Particles. In O. E. Wurl (Ed.), *Practical Guidelines for*
590 *the Analysis of Seawater*. CRC Press. <https://doi.org/doi:10.1201/9781420073072.ch7>
- 591 Engel, A., Bange, H. W., Cunliffe, M., Burrows, S. M., Friedrichs, G., Galgani, L., Herrmann, H.,
592 Hertkorn, N., Johnson, M., Liss, P. S., Quinn, P. K., Schartau, M., Soloviev, A., Stolle, C.,
593 Upstill-Goddard, R. C., van Pinxteren, M., & Zäncker, B. (2017). The Ocean's Vital Skin:
594 Toward an Integrated Understanding of the Sea Surface Microlayer. *Front. Mar. Sci.*, 4(165).
595 <https://doi.org/10.3389/fmars.2017.00165>
- 596 Engel, A., Borchard, C., Piontek, J., Schulz, K. G., Riebesell, U., & Bellerby, R. (2013). CO₂ increases
597 ¹⁴C primary production in an Arctic plankton community. *Biogeosciences*, 10(3), 1291-1308.
598 <https://doi.org/10.5194/bg-10-1291-2013>
- 599 Engel, A., & Galgani, L. (2016). The organic sea-surface microlayer in the upwelling region off the
600 coast of Peru and potential implications for air–sea exchange processes. *Biogeosciences*, 13(4),
601 989-1007. <https://doi.org/10.5194/bg-13-989-2016>
- 602 Engel, A., Sperling, M., Sun, C., Grosse, J., & Friedrichs, G. (2018). Organic Matter in the Surface
603 Microlayer: Insights From a Wind Wave Channel Experiment. *Front. Mar. Sci.*, 5(182).
604 <https://doi.org/10.3389/fmars.2018.00182>

605 Engel, A., Thoms, S., Riebesell, U., Rochelle-Newall, E., & Zondervan, I. (2004). Polysaccharide
606 aggregation as a potential sink of marine dissolved organic carbon. *Nature*, *428*(6986), 929-
607 932. <https://doi.org/https://doi.org/10.1038/nature02453>

608 Frew, N. M. (1997). The role of organic films in air–sea gas exchange. In P. S. Liss & R. A. Duce
609 (Eds.), *The Sea Surface and Global Change* (pp. 121-172). Cambridge University Press.
610 [https://doi.org/DOI: 10.1017/CBO9780511525025.006](https://doi.org/DOI:10.1017/CBO9780511525025.006)

611 Galgani, L., & Engel, A. (2016). Changes in optical characteristics of surface microlayers hint to
612 photochemically and microbially mediated DOM turnover in the upwelling region off the coast
613 of Peru. *Biogeosciences*, *13*(8), 2453-2473. <https://doi.org/10.5194/bg-13-2453-2016>

614 Galgani, L., Engel, A., Rossi, C., Donati, A., & Loiselle, S. A. (2018). Polystyrene microplastics
615 increase microbial release of marine Chromophoric Dissolved Organic Matter in microcosm
616 experiments. *Sci. Rep.*, *8*(1), 14635. <https://doi.org/10.1038/s41598-018-32805-4>

617 Galgani, L., Gossmann, I., Scholz-Böttcher, B., Jiang, X., Liu, Z., Scheidemann, L., Schlundt, C., and
618 Engel, A. (2022). Hitchhiking into the Deep: How Microplastic Particles are Exported through
619 the Biological Carbon Pump in the North Atlantic Ocean. *Environ. Sci. Technol.*,
620 <https://doi.org/10.1021/acs.est.2c04712> (in press)

621 Galgani, L., & Loiselle, S. A. (2019). Plastic Accumulation in the Sea Surface Microlayer: An
622 Experiment-Based Perspective for Future Studies. *Geosciences*, *9*.
623 <https://doi.org/https://doi.org/10.3390/geosciences9020066>

624 Galgani, L., & Loiselle, S. A. (2021). Plastic pollution impacts on marine carbon biogeochemistry.
625 *Environ. Pollut.*, *268*, 115598. <https://doi.org/https://doi.org/10.1016/j.envpol.2020.115598>

626 Galgani, L., Stolle, C., Endres, S., Schulz, K. G., & Engel, A. (2014). Effects of ocean acidification on
627 the biogenic composition of the sea-surface microlayer: Results from a mesocosm study. *J.*
628 *Geophys. Res.: Oceans*, *119*(11), 7911-7924. <https://doi.org/10.1002/2014jc010188>

629 Galgani, L., Tsapakis, M., Pitta, P., Tsiola, A., Tzempelikou, E., Kalantzi, I., Esposito, C., Loiselle, A.,
630 Tsotskou, A., Zivanovic, S., Dafnomili, E., Diliberto, S., Mylona, K., Magiopoulos, I., Zeri, C.,
631 Pitta, E., & Loiselle, S. A. (2019). Microplastics increase the marine production of particulate
632 forms of organic matter. *Environ. Res. Lett.* [https://doi.org/https://doi.org/10.1088/1748-](https://doi.org/https://doi.org/10.1088/1748-9326/ab59ca)
633 [9326/ab59ca](https://doi.org/https://doi.org/10.1088/1748-9326/ab59ca)

634 Garrett, W. D. (1965). Collection of Slick-forming Materials from the Sea Surface. *Limnol. Oceanogr.*,
635 *10*, 602-605. <https://doi.org/https://doi.org/10.4319/lo.1965.10.4.0602>

636 GESAMP (2019). *Guidelines or the monitoring and assessment of plastic litter and microplastics in*
637 *the ocean* (Kershaw P.J., Turra A. and Galgani F. editors), (IMO/FAO/UNESCO-
638 IOC/UNIDO/WMO/IAEA/UN/UNEP/UNDP/ISA Joint Group of Experts on the Scientific
639 Aspects of Marine Environmental Protection). Rep. Stud. GESAMP No. 99, 130p.

640 Gupta, K. K., & Devi, D. (2020). Characteristics investigation on biofilm formation and biodegradation
641 activities of *Pseudomonas aeruginosa* strain ISJ14 colonizing low density polyethylene (LDPE)
642 surface. *Heliyon*, *6*(7), e04398. <https://doi.org/https://doi.org/10.1016/j.heliyon.2020.e04398>

643 Han, Y. N., Wei, M., Han, F., Fang, C., Wang, D., Zhong, Y. J., Guo, C. L., Shi, X. Y., Xie, Z. K., &
644 Li, F. M. (2020). Greater Biofilm Formation and Increased Biodegradation of Polyethylene
645 Film by a Microbial Consortium of *Arthrobacter* sp. and *Streptomyces* sp. *Microorganisms*,
646 *8*(12). <https://doi.org/10.3390/microorganisms8121979>

647 Harlay, J., De Bodt, C., Engel, A., Jansen, S., d'ÂHoop, Q., Piontek, J., Van Oostende, N., Groom, S.,
648 Sabbe, K., & Chou, L. (2009). Abundance and size distribution of transparent exopolymer
649 particles (TEP) in a coccolithophorid bloom in the northern Bay of Biscay. *Deep Sea Res. Part*
650 *I Oceanogr. Res. Pap.*, *56*(8), 1251-1265. <https://doi.org/10.1016/j.dsr.2009.01.014>

651 Helms, J. R., Stubbins, A., Ritchie, J. D., Minor, E. C., Kieber, D. J., & Mopper, K. (2008). Absorption
652 spectral slopes and slope ratios as indicators of molecular weight, source, and photobleaching

653 of chromophoric dissolved organic matter. *Limnol. Oceanogr.*, 53(3), 955-969.
654 <https://doi.org/https://doi.org/10.4319/lo.2008.53.3.0955>

655 Hepach, H., Quack, B., Tegtmeier, S., Engel, A., Bracher, A., Fuhlbrügge, S., Galgani, L., Atlas, E. L.,
656 Lampel, J., Frieß, U., & Krüger, K. (2016). Biogenic halocarbons from the Peruvian upwelling
657 region as tropospheric halogen source. *Atmos. Chem. Phys.*, 16(18), 12219-12237.
658 <https://doi.org/10.5194/acp-16-12219-2016>

659 Hwang, J., Choi, D., Han, S., Jung, S. Y., Choi, J., & Hong, J. (2020). Potential toxicity of polystyrene
660 microplastic particles. *Sci. Rep.*, 10(1), 7391. <https://doi.org/10.1038/s41598-020-64464-9>

661 Jardillier, L., Zubkov, M. V., Pearman, J., & Scanlan, D. J. (2010). Significant CO₂ fixation by small
662 prymnesiophytes in the subtropical and tropical northeast Atlantic Ocean. *ISME J.*, 4(9), 1180-
663 1192. <https://doi.org/10.1038/ismej.2010.36>

664 Johnson, K. M., Dickson, A. G., Eiseheid, G., Goyet, C., Guenther, P., Key, R. M., Millero, F. J.,
665 Purkerson, D., Sabine, C. L., Schottle, R. G., Wallace, D. W. R., Wilke, R. J., & Winn, C. D.
666 (1998). Coulometric total carbon dioxide analysis for marine studies: assessment of the quality
667 of total inorganic carbon measurements made during the US Indian Ocean CO₂ Survey 1994–
668 1996. *Mar. Chem.*, 63(1), 21-37. [https://doi.org/https://doi.org/10.1016/S0304-](https://doi.org/https://doi.org/10.1016/S0304-4203(98)00048-6)
669 [4203\(98\)00048-6](https://doi.org/https://doi.org/10.1016/S0304-4203(98)00048-6)

670 Kvale, K., Prowe, A. E. F., Chien, C. T., Landolfi, A., & Oschlies, A. (2021). Zooplankton grazing of
671 microplastic can accelerate global loss of ocean oxygen. *Nat. Commun.*, 12(1), 2358.
672 <https://doi.org/10.1038/s41467-021-22554-w>

673 Lear, G., Kingsbury, J. M., Franchini, S., Gambarini, V., Maday, S. D. M., Wallbank, J. A., Weaver,
674 L., & Pantos, O. (2021). Plastics and the microbiome: impacts and solutions. *Environmental*
675 *Microbiome*, 16(1), 2. <https://doi.org/10.1186/s40793-020-00371-w>

- 676 Lee, Y. K., Murphy, K. R., & Hur, J. (2020). Fluorescence Signatures of Dissolved Organic Matter
677 Leached from Microplastics: Polymers and Additives. *Environ. Sci. Technol.*, *54*(19), 11905-
678 11914. <https://doi.org/10.1021/acs.est.0c00942>
- 679 Lindgren, J. F., Wilewska-Bien, M., Granhag, L., Andersson, K., & Eriksson, K. M. (2016). Discharges
680 to the Sea. In K. Andersson, S. Brynolf, J. F. Lindgren, & M. Wilewska-Bien (Eds.), *Shipping
681 and the Environment : Improving Environmental Performance in Marine Transportation* (pp.
682 125-168). Springer Berlin Heidelberg. https://doi.org/10.1007/978-3-662-49045-7_4
- 683 Liss, P. S., & Duce, R. A. (2005). *The Sea Surface and Global Change*. Cambridge University Press.
684 <https://doi.org/doi:10.1017/CBO9780511525025>
- 685 Loiselle, S. A., Bracchini, L., Dattilo, A. M., Ricci, M., Tognazzi, A., Cózar, A., & Rossi, C. (2009).
686 The optical characterization of chromophoric dissolved organic matter using wavelength
687 distribution of absorption spectral slopes. *Limnol. Oceanogr.*, *54*(2), 590-597.
688 <https://doi.org/10.4319/lo.2009.54.2.0590>
- 689 Lueker, T. J., Dickson, A. G., & Keeling, C. D. (2000). Ocean pCO₂ calculated from dissolved
690 inorganic carbon, alkalinity, and equations for K₁ and K₂: validation based on laboratory
691 measurements of CO₂ in gas and seawater at equilibrium. *Mar. Chem.*, *70*(1), 105-119.
692 [https://doi.org/https://doi.org/10.1016/S0304-4203\(00\)00022-0](https://doi.org/https://doi.org/10.1016/S0304-4203(00)00022-0)
- 693 Mari, X. (1999). Carbon content and C:N ratio of transparent exopolymeric particles (TEP) produced
694 by bubbling exudates of diatoms. *Mar. Ecol. Prog. Ser.*, *183*, 59-71.
695 <https://doi.org/10.3354/meps183059>
- 696 Mari, X., & Burd, A. (1998). Seasonal size spectra of transparent exopolymeric particles (TEP) in a
697 coastal sea and comparison with those predicted using coagulation theory. *Mar. Ecol. Prog.
698 Ser.*, *163*, 63-76. <https://doi.org/10.3354/meps163063>

699 Mari, X., & Kiørboe, T. (1996). Abundance, size distribution and bacterial colonization of transparent
700 exopolymeric particles (TEP) during spring in the Kattegat. *J. Plankton Res.*, 18(6), 969-986.
701 <https://doi.org/10.1093/plankt/18.6.969>

702 Marie, D., Partensky, F., Jacquet, S., & Vaultot, D. (1997). Enumeration and Cell Cycle Analysis of
703 Natural Populations of Marine Picoplankton by Flow Cytometry Using the Nucleic Acid Stain
704 SYBR Green I. *Appl. Environ. Microbiol.*, 63(1), 186-193.
705 <https://doi.org/https://doi.org/10.1128/aem.63.1.186-193.1997>

706 Michels, J., Stippkugel, A., Lenz, M., Wirtz, K., & Engel, A. (2018). Rapid aggregation of biofilm-
707 covered microplastics with marine biogenic particles. *Proc. Royal Soc. B.*
708 <https://doi.org/http://dx.doi.org/10.1098/rspb.2018.1203>

709 Mintrop, L., Pérez, F. F., González-Dávila, M., Santana-Casiano, J. M., & Körtzinger, A. (2000).
710 Alkalinity determination by potentiometry: intercalibration using three different methods.
711 *Cienc. Mar.*, 26(1), 23-27. <https://doi.org/http://dx.doi.org/10.7773/cm.v26i1.573>

712 Mustaffa, N. I. H., Ribas-Ribas, M., Banko-Kubis, H. M., & Wurl, O. (2020). Global reduction of in
713 situ CO₂ transfer velocity by natural surfactants in the sea-surface microlayer. *Proc. Math.*
714 *Phys. Eng. Sci.*, 476(2234), 20190763. <https://doi.org/10.1098/rspa.2019.0763>

715 Orr, J. C., Epitalon, J. M., & Gattuso, J. P. (2015). Comparison of ten packages that compute ocean
716 carbonate chemistry. *Biogeosciences*, 12(5), 1483-1510. [https://doi.org/10.5194/bg-12-1483-](https://doi.org/10.5194/bg-12-1483-2015)
717 2015

718 Ortega-Retuerta, E., Mazuecos, I. P., Reche, I., Gasol, J. M., Álvarez-Salgado, X. A., Álvarez, M.,
719 Montero, M. F., & Arístegui, J. (2019). Transparent exopolymer particle (TEP) distribution and
720 in situ prokaryotic generation across the deep Mediterranean Sea and nearby North East
721 Atlantic Ocean. *Prog. Oceanogr.*, 173, 180-191.
722 <https://doi.org/https://doi.org/10.1016/j.pocean.2019.03.002>

723 Pabortsava, K., & Lampitt, R. S. (2020). High concentrations of plastic hidden beneath the surface of
724 the Atlantic Ocean. *Nat. Comm.*, *11*(1), 4073. <https://doi.org/10.1038/s41467-020-17932-9>

725 Paerl, H. W. (1975). Microbial attachment to particles in marine and freshwater ecosystems. *Microb.*
726 *Ecol.*, *2*(1), 73-83. <https://doi.org/10.1007/bf02010382>

727 Pierrot, D., Lewis, E., & Wallace, D. W. R. (2006). MS Excel Program Developed for CO2 System
728 Calculations. ORNL/CDIAC-105a. Carbon Dioxide Information Analysis Center, Oak Ridge
729 National Laboratory, U.S. Department of Energy, Oak Ridge, Tennessee. doi:
730 10.3334/CDIAC/otg.CO2SYS_XLS_CDIAC105a

731 Pitta, P., Nejstgaard, J. C., Tsagaraki, T. M., Zervoudaki, S., Egge, J. K., Frangoulis, C., Lagaria, A.,
732 Magiopoulos, I., Psarra, S., Sandaa, R.-A., Skjoldal, E. F., Tanaka, T., Thyrrhaug, R., &
733 Thingstad, T. F. (2016). Confirming the “Rapid phosphorus transfer from microorganisms to
734 mesozooplankton in the Eastern Mediterranean Sea” scenario through a mesocosm experiment.
735 *J. Plankton Res.*, *38*(3), 502-521. <https://doi.org/10.1093/plankt/fbw010>

736 Rahav, E., Shun-Yan, C., Cui, G., Liu, H., Tsagaraki, T. M., Giannakourou, A., Tsiola, A., Psarra, S.,
737 Lagaria, A., Mulholland, M. R., Stathopoulou, E., Paraskevi, P., Herut, B., & Berman-Frank,
738 I. (2016). Evaluating the Impact of Atmospheric Depositions on Springtime Dinitrogen
739 Fixation in the Cretan Sea (Eastern Mediterranean)—A Mesocosm Approach. *Front. Mar. Sci.*,
740 *3*. <https://doi.org/10.3389/fmars.2016.00180>

741 Rahlff, J., Stolle, C., Giebel, H.-A., Brinkhoff, T., Ribas-Ribas, M., Hodapp, D., & Wurl, O. (2017).
742 High wind speeds prevent formation of a distinct bacterioneuston community in the sea-surface
743 microlayer. *FEMS Microbiol. Ecol.*, *93*(5), fix041-fix041.
744 <https://doi.org/10.1093/femsec/fix041>

- 745 Rahlff, J., Stolle, C., Giebel, H.-A., Ribas-Ribas, M., Damgaard, L. R., & Wurl, O. (2019). Oxygen
746 Profiles Across the Sea-Surface Microlayer—Effects of Diffusion and Biological Activity.
747 *Front. Mar. Sci.*, 6(11). <https://doi.org/10.3389/fmars.2019.00011>
- 748 Romera-Castillo, C., Birnstiel, S., Álvarez-Salgado, X. A., & Sebastián, M. (2022). Aged Plastic
749 Leaching of Dissolved Organic Matter Is Two Orders of Magnitude Higher Than Virgin Plastic
750 Leading to a Strong Uplift in Marine Microbial Activity. *Front. Mar. Sci* 9 :861557.
751 <https://doi.org/10.3389/fmars.2022.861557>
- 752 Romera-Castillo, C., Mallenco-Fornies, R., Saá-Yáñez, M., & Álvarez-Salgado, X. A. (2022). Leaching
753 and bioavailability of dissolved organic matter from petrol-based and biodegradable plastics.
754 *Mar. Environ. Res.*, 176, 105607. <https://doi.org/10.1016/j.marenvres.2022.105607>
- 755 Royer, S.-J., Ferrón, S., Wilson, S. T., & Karl, D. M. (2018). Production of methane and ethylene from
756 plastic in the environment. *PLOS ONE*, 13(8), e0200574.
757 <https://doi.org/10.1371/journal.pone.0200574>
- 758 Santschi, P. H., Chin, W.-C., Quigg, A., Xu, C., Kamalanathan, M., Lin, P., & Shiu, R.-F. (2021).
759 Marine Gel Interactions with Hydrophilic and Hydrophobic Pollutants. *Gels*, 7(3), 83.
760 <https://www.mdpi.com/2310-2861/7/3/83>
- 761 Savoca, M. S., Wohlfeil, M. E., Ebeler, S. E., & Nevitt, G. A. (2016). Marine plastic debris emits a
762 keystone infochemical for olfactory foraging seabirds. *Sci. Adv.*, 2(11), e1600395.
763 <https://doi.org/doi:10.1126/sciadv.1600395>
- 764 Sharma, S., Sharma, V., & Chatterjee, S. (2021). Microplastics in the Mediterranean Sea: Sources,
765 Pollution Intensity, Sea Health, and Regulatory Policies. *Front. Mar. Sci*, 8.
766 <https://doi.org/10.3389/fmars.2021.634934>

- 767 Shen, M., Ye, S., Zeng, G., Zhang, Y., Xing, L., Tang, W., Wen, X., & Liu, S. (2020). Can microplastics
768 pose a threat to ocean carbon sequestration? *Mar. Pollut. Bull.*, *150*, 110712.
769 <https://doi.org/https://doi.org/10.1016/j.marpolbul.2019.110712>
- 770 Shiu, R.-F., Vazquez, C. I., Chiang, C.-Y., Chiu, M.-H., Chen, C.-S., Ni, C.-W., Gong, G.-C., Quigg,
771 A., Santschi, P. H., & Chin, W.-C. (2020). Nano- and microplastics trigger secretion of protein-
772 rich extracellular polymeric substances from phytoplankton. *Sci.Total. Environ.*, *748*, 141469.
773 <https://doi.org/https://doi.org/10.1016/j.scitotenv.2020.141469>
- 774 Su, X., Yang, L., Yang, K., Tang, Y., Wen, T., Wang, Y., Rillig, M. C., Rohe, L., Pan, J., Li, H., &
775 Zhu, Y.-g. (2022). Estuarine plastisphere as an overlooked source of N₂O production. *Nature*
776 *Communications*, *13*(1), 3884. <https://doi.org/10.1038/s41467-022-31584-x>
- 777 Thompson, J. B. (2000). Microbial Whittings. In R. E. Riding & S. M. Awramik (Eds.), *Microbial*
778 *Sediments* (pp. 250-260). Springer Berlin Heidelberg. [https://doi.org/10.1007/978-3-662-](https://doi.org/10.1007/978-3-662-04036-2_27)
779 [04036-2_27](https://doi.org/10.1007/978-3-662-04036-2_27)
- 780 Thompson, J. B., Schultze-Lam, S., Beveridge, T. J., & Des Marais, D. J. (1997). Whiting events:
781 biogenic origin due to the photosynthetic activity of cyanobacterial picoplankton. *Limnol.*
782 *Oceanogr.*, *42*(1), 133-141. <https://doi.org/10.4319/lo.1997.42.1.0133>
- 783 Thornton, D. C. O. (2018). Coomassie Stainable Particles (CSP): Protein Containing Exopolymer
784 Particles in the Ocean. *Front. Mar. Sci.*, *5*(206). <https://doi.org/10.3389/fmars.2018.00206>
- 785 Thornton, D. C. O., Brooks, S. D., & Chen, J. (2016). Protein and Carbohydrate Exopolymer Particles
786 in the Sea Surface Microlayer (SML). *Front. Mar. Sci.*, *3*(135).
787 <https://doi.org/10.3389/fmars.2016.00135>
- 788 Tsiola, A., Pitta, P., Callol, A. J., Kagiorgi, M., Kalantzi, I., Mylona, K., Santi, I., Toncelli, C., Pergantis,
789 S., & Tsapakis, M. (2017). The impact of silver nanoparticles on marine plankton dynamics:

790 Dependence on coating, size and concentration. *Sci. Total. Environ.*, 601-602, 1838-1848.
791 <https://doi.org/https://doi.org/10.1016/j.scitotenv.2017.06.042>

792 Tsiola, A., Tsagaraki, T. M., Giannakourou, A., Nikolioudakis, N., Yücel, N., Herut, B., & Pitta, P.
793 (2017). Bacterial Growth and Mortality after Deposition of Saharan Dust and Mixed Aerosols
794 in the Eastern Mediterranean Sea: A Mesocosm Experiment. *Front. Mar. Sci.*, 3.
795 <https://doi.org/10.3389/fmars.2016.00281>

796 Upstill-Goddard, R. C. (2006). Air–sea gas exchange in the coastal zone. *Estuar. Coast. Shelf Sci.*,
797 70(3), 388-404. <https://doi.org/https://doi.org/10.1016/j.ecss.2006.05.043>

798 Verdugo, P. (2012). Marine Microgels. *Ann. Rev. Mar. Sci.*, 4(1), 375-400.
799 <https://doi.org/doi:10.1146/annurev-marine-120709-142759>

800 Wurl, O., Ekau, W., Landing, W. M., & Zappa, C. J. (2017). Sea surface microlayer in a changing ocean
801 – A perspective. *Elementa-Sci. Anthropol.*, 5(31).
802 <https://doi.org/http://doi.org/10.1525/elementa.228>

803 Wurl, O., & Holmes, M. (2008). The gelatinous nature of the sea-surface microlayer. *Mar. Chem.*,
804 110(1-2), 89-97. <https://doi.org/10.1016/j.marchem.2008.02.009>

805 Wurl, O., Stolle, C., Van Thuoc, C., The Thu, P., & Mari, X. (2016). Biofilm-like properties of the sea
806 surface and predicted effects on air–sea CO₂ exchange. *Prog. Oceanogr.*, 144, 15-24.
807 <https://doi.org/https://doi.org/10.1016/j.pocean.2016.03.002>

808 Yue, W.-z., Sun, C.-c., Shi, P., Engel, A., Wang, Y.-s., & He, W.-H. (2018). Effect of temperature on
809 the accumulation of marine biogenic gels in the surface microlayer near the outlet of nuclear
810 power plants and adjacent areas in the Daya Bay, China. *PLOS ONE*, 13(6), e0198735.
811 <https://doi.org/10.1371/journal.pone.0198735>

- 812 Zäncker, B., Bracher, A., Röttgers, R., & Engel, A. (2017). Variations of the Organic Matter
813 Composition in the Sea Surface Microlayer: A Comparison between Open Ocean, Coastal, and
814 Upwelling Sites Off the Peruvian Coast. *Front. Microbiol.* , 8(2369).
815 <https://doi.org/10.3389/fmicb.2017.02369>
- 816 Zäncker, B., Cunliffe, M., & Engel, A. (2018). Bacterial Community Composition in the Sea Surface
817 Microlayer Off the Peruvian Coast. *Front. Microbiol.* , 9(2699).
818 <https://doi.org/10.3389/fmicb.2018.02699>
- 819 Zettler, E. R., Mincer, T. J., & Amaral-Zettler, L. A. (2013). Life in the “Plastisphere”: Microbial
820 Communities on Plastic Marine Debris. *Environ. Sci. Technol.*, 47(13), 7137-7146.
821 <https://doi.org/10.1021/es401288x>
- 822 Zhao, S., Zettler, E. R., Amaral-Zettler, L. A., & Mincer, T. J. (2021). Microbial carrying capacity and
823 carbon biomass of plastic marine debris. *ISME J.*, 15(1), 67-77. [https://doi.org/10.1038/s41396-](https://doi.org/10.1038/s41396-020-00756-2)
824 [020-00756-2](https://doi.org/10.1038/s41396-020-00756-2)

825 **Figures and Tables**

826

827

828

829

830

831

832

833

834

835

Parameter / unit	ANOVA F	P value	Test	Mean Control	Mean MP	SE of difference	% of difference MP-C
TA (ULW) [$\mu\text{mol Kg}^{-1}$]	F (11, 43) = 3.138	0.0035	REML	2625.0	2631.0	1.77	0.2
DIC (ULW)* [$\mu\text{mol Kg}^{-1}$]	F (11, 43) = 9.482	<0.0001	REML (time)	2283.0	2286.0	0.94	0.1
pCO ₂ (ULW) [μatm]	F (11, 43) = 4.279	0.0003	REML	420.20	409.10	3.78	-2.6
pH (ULW)	F (11, 43) = 4.552	0.0001	REML	8.064	8.075	0.00	0.14
CO ₃ ²⁻ (ULW) [$\mu\text{mol Kg}^{-1}$]	F (11, 43) = 2.814	0.0075	REML	243.10	246.20	1.09	1.3
CO ₂ (ULW) [$\mu\text{mol Kg}^{-1}$]	F (11, 43) = 3.845	0.0007	REML	13.09	12.78	0.11	-2.4
HCO ₃ ⁻ (ULW) [$\mu\text{mol Kg}^{-1}$]	F (11, 43) = 2.991	0.0049	REML (time)	2027.0	2027.0	1.27	0.0
TEP (SML)* [10 ⁶ mm ² L ⁻¹]	F (6, 24) = 3.573	0.0113	RM ANOVA (time)	493.50	641.70	60.30	30.0
TEP (SML) [10 ⁶ particles L ⁻¹]	F (6, 24) = 2.836	0.0312	RM ANOVA	61.06	77.44	5.53	26.8
TEP-C (SML)* [$\mu\text{g Carbon L}^{-1}$]	F (6, 24) = 3.868	0.0077	RM ANOVA (time)	324.30	424.80	49.43	31.0
CSP (SML) [10 ⁶ mm ² L ⁻¹]	F (6, 24) = 4.932	0.002	RM ANOVA	682.30	854.50	55.72	25.2
CSP (SML) [10 ⁶ particles L ⁻¹]	F (6, 24) = 4.870	0.0022	RM ANOVA	75.93	113.57	8.24	49.6
Syn (SML) [10 ⁶ cells L ⁻¹]	F (5, 20) = 4.417	0.0071	RM ANOVA	64.28	65.15	3.01	1.4
HDNA-Syn (SML)* [10 ⁶ cells L ⁻¹]	F (5, 20) = 21.54	<0.0001	RM ANOVA (time)	1.46	1.81	0.22	23.5
LDNA-Syn (SML) [10 ⁶ cells L ⁻¹]	F (5, 20) = 4.947	0.0041	RM ANOVA	62.85	63.35	2.84	0.8
S ₂₇₅₋₂₉₅ (SML) [nm ⁻¹]	F (6, 24) = 3.146	0.0203	RM ANOVA	0.01	0.01	0.00	4.1
a(355) nm (SML) [m ⁻¹]	F (6, 24) = 1.090	0.3963	RM ANOVA	3.89	3.90	0.05	0.1
DOC (SML) [mg L ⁻¹]	F (1, 4) = 0.02581	0.6927	REML	1.23	1.21	0.11	-1.5
H. Bacteria (SML)* [10 ⁸ cells L ⁻¹]	F (6, 21) = 9.815	<0.0001	REML (time)	4.46	4.31	0.42	-3.4
HDNA H. Bacteria (SML)* [10 ⁸ cells L ⁻¹]	F (6, 21) = 10.40	<0.0001	REML (time)	3.13	2.98	0.39	-4.8
LDNA H. Bacteria (SML)* [10 ⁸ cells L ⁻¹]	F (6, 21) = 13.07	<0.0001	REML (time)	1.27	1.34	0.05	5.3

836

837 **Table 1** Repeated Measures Two-Way ANOVA or Mixed effects Model (REML) Analysis Table

838 where the fixed factor is the “treatment” (MP/ no MP) and the random effect is the time.

839 Results are shown as the interaction of “treatment x time” unless otherwise noted. Replicates

840 within the treatments have been assumed having equal variability of differences. (*) indicates

841 differences that have been observed between MP and Control in time. Significant differences
 842 are accepted for $p < 0.05$.

843 SML = sea-surface microlayer; ULW = underlying water; TA = Total Alkalinity; DIC =
 844 Dissolved Inorganic Carbon; TEP = Transparent Exopolymer Particles; TEP-C = Carbon
 845 contained in Transparent Exopolymer Particles; CSP = Coomassie Stainable Particles; Syn
 846 =Synechococcus cells; HDNA-Syn = high DNA containing Synechococcus cells; LDNA-Syn =
 847 low DNA containing Synechococcus cells; $S_{275-295}$ = Spectral Slope measured between 275 and
 848 295 nm; $a(355)$ = CDOM (Chromophoric Dissolved Organic Matter) absorption coefficient at
 849 355 nm; DOC =Dissolved organic Carbon; H.Bacteria = Heterotrophic Bacteria; HDNA H.
 850 Bacteria = high DNA containing heterotrophic bacterial cells; LDNA H. Bacteria = low DNA
 851 containing heterotrophic bacterial cells.

$S_{275-295}$ [nm^{-1}], SML	$p\text{CO}_2$ [μatm], ULW	DOC [mg L^{-1}], SML	Heterotrophic bacteria [cells L^{-1}], SML	CSP [$\text{mm}^2 \text{L}^{-1}$], SML	Synechococcus [cells L^{-1}], SML
Spearman r	0.51	0.45	0.34	0.35	-0.61
p	< 0.001	0.004	0.032	0.024	< 0.0001
n	42	39	39	42	39

852
 853 **Table 2** Spearman r correlation table reporting significant correlations of Spectral Slope
 854 parameter in the SML (sea-surface microlayer) between 275 and 295 nm ($S_{275-295}$) to $p\text{CO}_2$
 855 (ulw), and DOC, Heterotrophic Bacteria, CSP and Synechococcus cells in the SML. DOC
 856 =Dissolved organic Carbon; CSP = Coomassie Stainable Particles.

857
 858
 859
 860
 861
 862
 863
 864
 865

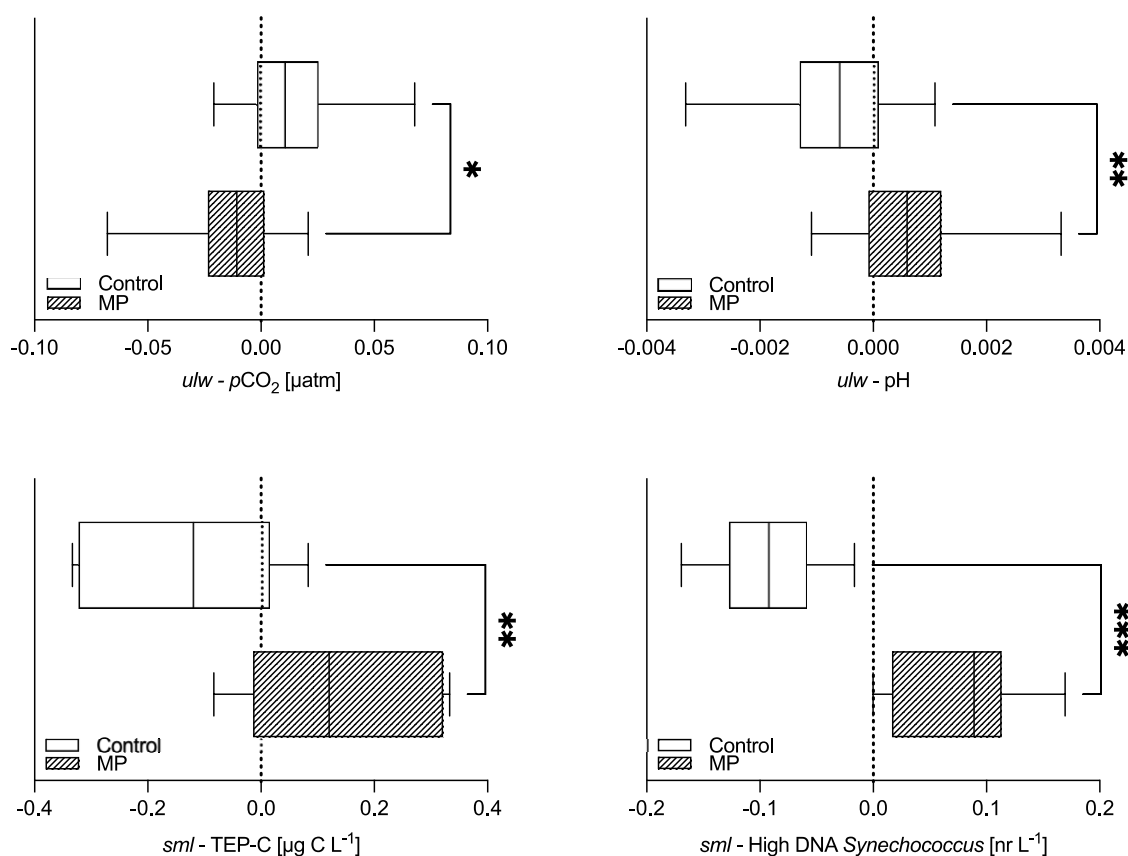
<i>Synechococcus</i> [cells L ⁻¹]	TA [μmol Kg ⁻¹]	DIC [μmol Kg ⁻¹]	pH in	pCO ₂ [μatm]	CO ₃ ²⁻ [μmol Kg ⁻¹]	CO ₂ [μmol Kg ⁻¹]
<i>Spearman r</i>	0.531	0.429	0.344	-0.33	0.336	-0.321
<i>p</i>	0.000557	0.00664	0.0323	0.0406	0.0368	0.0465
<i>n</i>	39	39	39	39	39	39

TEP-C [μg C L ⁻¹]	TA [μmol Kg ⁻¹]	DIC [μmol Kg ⁻¹]	pH in	pCO ₂ [μatm]	CO ₃ ²⁻ [μmol Kg ⁻¹]	CO ₂ [μmol Kg ⁻¹]
<i>Spearman r</i>	0.511	0.273	0.434	-0.433	0.481	-0.437
<i>p</i>	0.000592	0.0798	0.00428	0.00438	0.00137	0.00395
<i>n</i>	42	42	42	42	42	42

866

867 **Table 3** Spearman *r* correlation table between *Synechococcus* and Carbon contained in
868 Transparent Exopolymer Particles (TEP-C) in the SML (sea-surface microlayer), to Total
869 Alkalinity (TA), Dissolved Inorganic Carbon (DIC), pH, pCO₂ CO₃²⁻ and CO₂ in the underlying
870 water of the mesocosms.

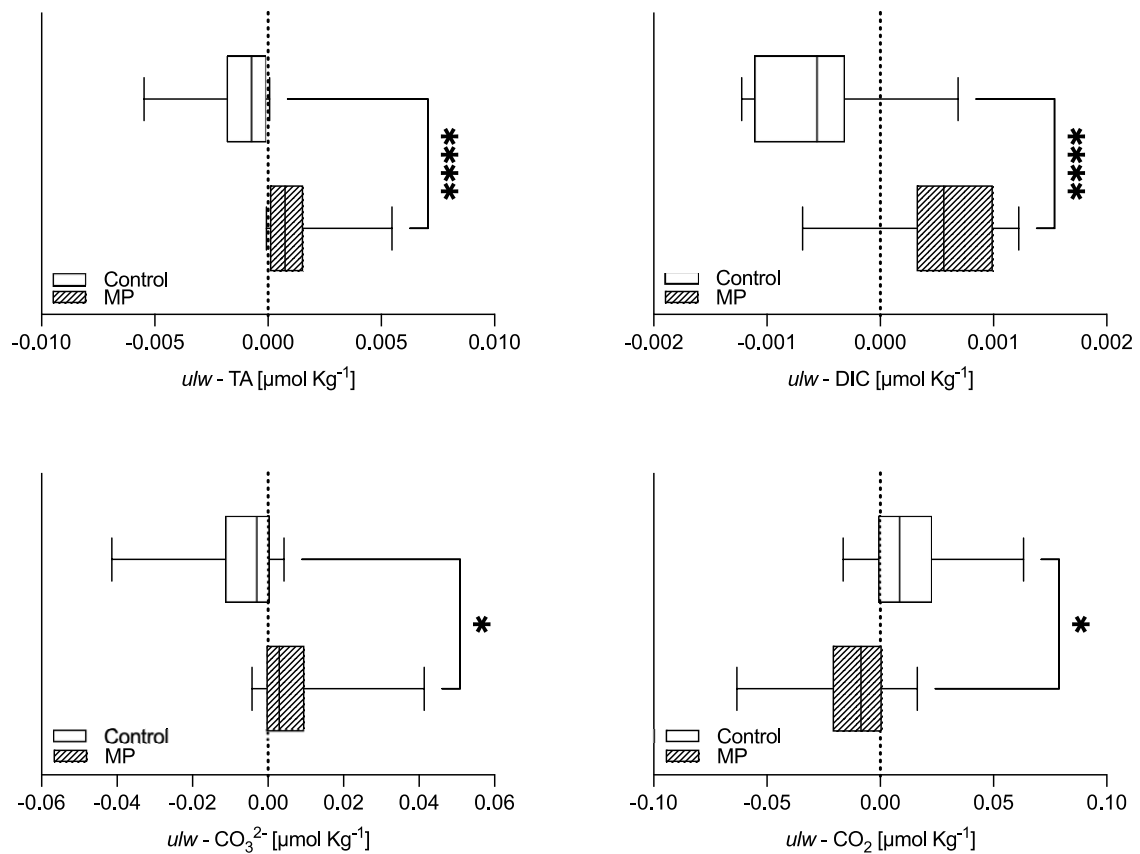
871



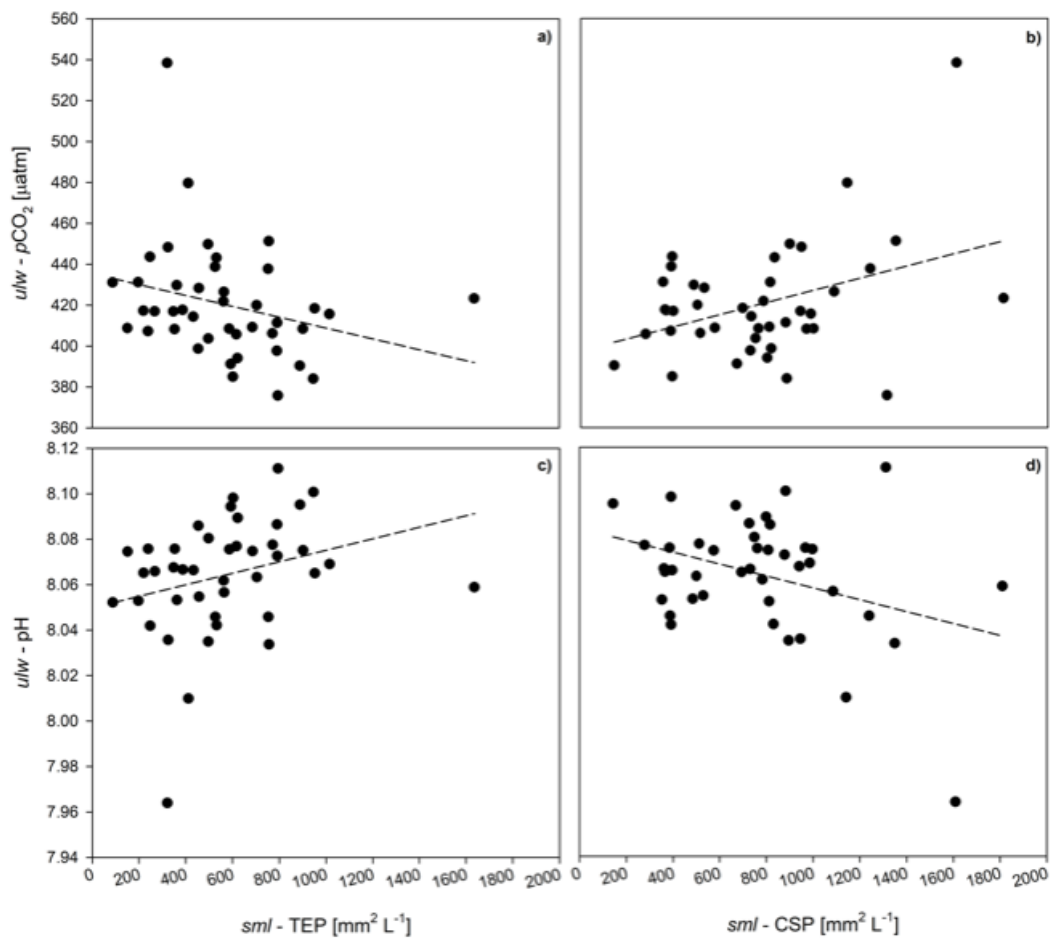
872

873 **Figure 1** Boxplots represent normalized anomalies and 5-95 percentiles for underlying water
874 (ulw) pCO₂, pH, and for sea-surface microlayer (SML) Carbon contained in Transparent

875 *Exopolymer Particles (TEP-C) and High DNA containing Synechococcus cells. Stars indicate*
 876 *the level of significance in the differences between control and MP mesocosms based on Mann-*
 877 *Whitney tests on normalized anomalies (pCO₂, pH), and unpaired t-tests (TEP-C and High*
 878 *DNA Synechococcus cells).*



879
 880 **Figure 2** Boxplots that represent normalized anomalies and 5-95 percentiles for underlying
 881 water (*ulw*) Total Alkalinity (TA), Dissolved Inorganic Carbon (DIC), CO₃²⁻ and CO₂. Stars
 882 indicate the level of significance in the differences between control and MP mesocosms based
 883 on Mann-Whitney test (TA, CO₃²⁻ and CO₂) and unpaired t-test (DIC).



884

885 **Figure 3** Panels a, b: Multiple linear regression between pCO_2 in the underlying water (ulw)
 886 and the presence of marine gels (TEP, a; CSP, b) in the sea-surface microlayer (SML).

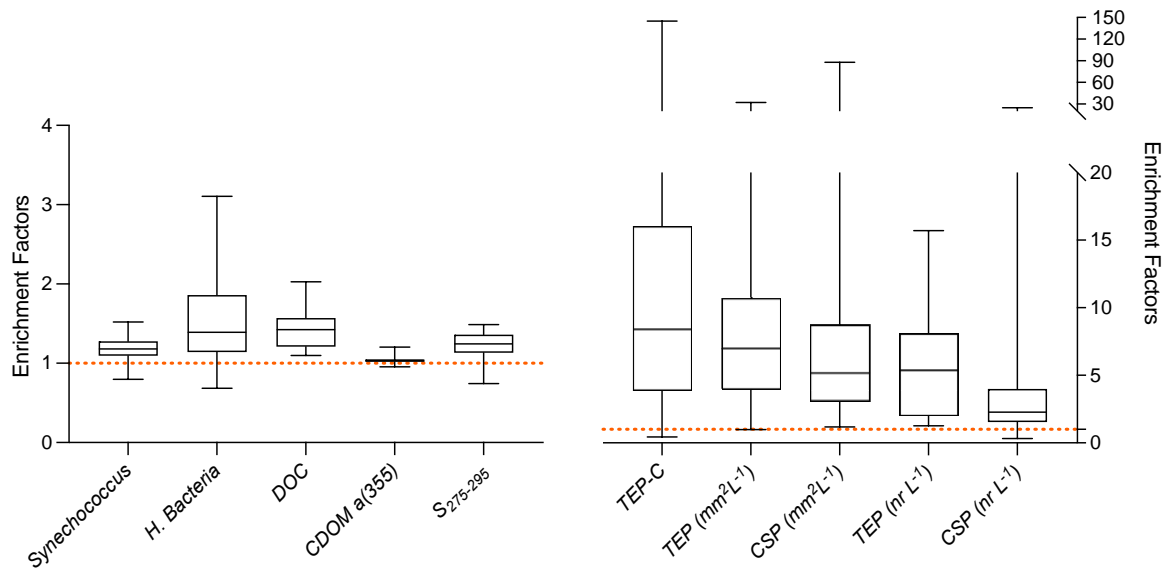
887 Panels c, d: Multiple linear regression between pH in the underlying water (ulw) on marine
 888 gels (TEP, c; CSP, d) in the sea-surface microlayer (SML) according to the equation:

889
$$pH = 8.070 + 0.0000471 \text{ TEP } [mm^2 \text{ L}^{-1}] - 0.0000421 \text{ CSP } [mm^2 \text{ L}^{-1}].$$

890 For the regression, $R^2 = 0.365$, $p < 0.001$, $F = 11.22$, $DF = 2$. All panels have been displayed
 891 separately to better visualize the trends. TEP = Transparent Exopolymer Particles; CSP =
 892 Coomassie Stainable Particles.

893

894



895

896 **Figure 4** Enrichment factors (EF) for sea-surface microlayer (SML) parameters compared to
 897 underlying water independently from the treatments (all data from control and MP

898 mesocosms are merged). The dashed orange line is set on both graphs to $EF = 1$ which

899 means no real differences between SML concentration and underlying water concentration.

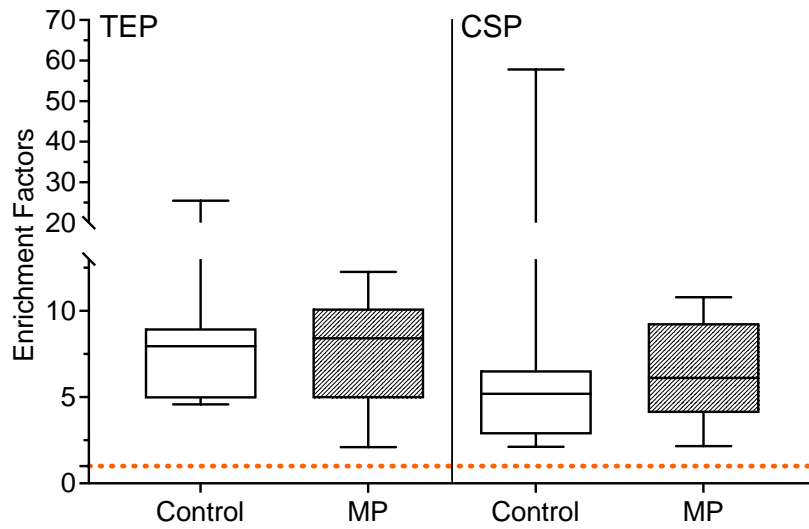
900 *H. Bacteria* = heterotrophic bacteria; *DOC* = Dissolved Organic Carbon; *CDOM a(355)* =

901 Chromophoric Dissolved Organic Matter absorption coefficient at 355 nm; *S₂₇₅₋₂₉₅* = Spectral

902 Slope measured between 275 and 295 nm; *TEP* = Transparent Exopolymer Particles; *TEP-C*

903 = Carbon contained in Transparent Exopolymer Particles; *CSP* = Coomassie Stainable

904 Particles.



905

906 **Figure 5** Enrichment Factors for the concentration of marine gels TEP and CSP, expressed
 907 as $\text{area mm}^2 \text{ L}^{-1}$, between Control and MP mesocosms. The orange dashed line indicates EF

908 = 1. Repeated Measures two-way ANOVA tests (Table S1) have evidenced significant

909 differences between EFs for marine gels. TEP = Transparent Exopolymer Particles; CSP =

910 Coomassie Stainable Particles.